Journal of Archaeological Science 171 (2024) 106088

Contents lists available at ScienceDirect

Journal of Archaeological Science

journal homepage: www.elsevier.com/locate/jas

Reconstructing infant mortality in Iberian Iron Age populations from tooth histology

Ani Martirosyan [a,b], Carolina Sandoval-Ávila [a,b], Javier Irurita [c], Judith Juanhuix [d], Nuria Molist [e], Immaculada Mestres [f], Montserrat Durán [f], Natàlia Alonso [g], Cristina Santos [a,b], Assumpció Malgosa [a,b], Judit Molera [h], Xavier Jordana [a,i,*]

[a] *Biological Anthropology Unit, Department of Animal Biology, Plant Biology and Ecology, Faculty of Biosciences, Universitat Autònoma de Barcelona, Cerdanyola Del Vallès, 08193, Barcelona, Spain*
[b] *Research Group in Biological Anthropology (GREAB), Universitat Autònoma de Barcelona, Cerdanyola Del Vallès, 08193, Barcelona, Spain*
[c] *Department of Legal Medicine, Toxicology and Physical Anthropology, Universidad de Granada, 18071, Granada, Spain*
[d] *ALBA Synchrotron Light Facility, Cerdanyola Del Vallès, 08290, Barcelona, Spain*
[e] *Museu d'Arqueologia de Catalunya (MAC), Passeig de Santa Madrona 39-41, 080038, Barcelona, Spain*
[f] *Centre d'Interpretació El Camp de Les Lloses, Pau Casals, 2, 08551, Tona, Barcelona, Spain*
[g] *ARQHISTEC-GIP, Departament de Geografia, Història I Història de L'Art, Facultat de Lletres, Universitat de Lleida, Plaça de Victor Siurana, 1, 25003, Lleida, Spain*
[h] *MECAMAT, Universitat de Vic-Universitat Central de Catalunya, Campus Torre Dels Frares, 08500, Vic, Spain*
[i] *Tissue Repair and Regeneration Laboratory (TR2Lab), Institut de Recerca I Innovació en Ciències de La Vida I de La Salut a La Catalunya Central (IrisCC), Ctra. de Roda, 08500, Vic, Barcelona, Spain*

ARTICLE INFO

Keywords:
Neonatal line
Crown formation time
Synchrotron X-ray fluorescence
Deciduous teeth
Iberian culture

ABSTRACT

The Neonatal Line (NNL) of the tooth serves as a unique identifier, allowing us to distinguish whether a child survived birth. This line is essential for assessing the age at death of infants from skeletal remains found in archaeological contexts. Our primary objective is to accurately determine the age of infant intramural inhumations from the Iberian Iron Age (8th-1st centuries BC) by analyzing histological sections of tooth germs. Due to their fragility and high susceptibility to taphonomic factors, these samples are challenging to handle. By accurately assessing their age, we aim to classify individuals into various stages of infant mortality, which will help reconstruct infant mortality patterns in these populations.

We analyze unerupted and still-forming crown deciduous teeth from 45 infant burials. By calculating Crown Formation Time (CFT) and identifying the NNL, we determine both gestational and chronological ages. We further validate the reliability of NNL identification through Synchrotron X-ray Fluorescence (SXRF) elemental analysis (Ca, Zn, Cu) on two contemporary and two archaeological samples.

Our histological study reveals the chronological age of 38 infants from Iberian settlements, ranging from the 30th week of gestation to the 2nd postnatal month. The age distribution shows an attritional mortality pattern, with nearly half experiencing perinatal mortality, including preterm births. These findings support the hypothesis that mortality was primarily attributed to natural causes. Our research enhances the understanding of infant life history events in prehistory by combining histological analysis of tooth NNL and CFT, highlighting the technique's potential and limitations.

1. Introduction

Accurate age determination is paramount in the reconstruction of mortality profiles from archaeological human skeletal remains, particularly when focusing on infants within their initial year of life. The ability to reconstruct infant mortality rates serves as a critical indicator of overall societal health, offering essential insights into the well-being of both mothers and infants (Luke et al., 1993; Razzaque et al., 2022). Consequently, the precision of such reconstructions holds the key to unraveling past demographic events in human societies of antiquity.

* Corresponding author. Biological Anthropology Unit, Department of Animal Biology, Plant Biology and Ecology, Faculty of Biosciences, Universitat Autònoma de Barcelona, Cerdanyola Del Vallès, 08193, Barcelona, Spain.
E-mail address: xavier.jordana@uab.cat (X. Jordana).

https://doi.org/10.1016/j.jas.2024.106088
Received 8 July 2024; Received in revised form 18 September 2024; Accepted 25 September 2024
Available online 4 October 2024

Infant mortality encompasses various stages: perinatal, neonatal, and post-neonatal. Perinatal mortality is divided into two stages: stillbirth occurring after the 27th week of gestation, and early neonatal mortality, covering the first week of life (Monnier, 1985). Neonatal mortality includes early neonatal mortality and late neonatal mortality which occurs between the 8th and 28th day of life. Post-neonatal mortality spans from the 28th day to the end of the first year. These stages present different mortality risk factors and demand precise age determination, especially during the first month of life, which poses the highest risk of mortality (Jabeen et al., 2023; Pal et al., 2020).

Conventional anthropological methods (Cunningham et al., 2017) estimate developmental age at death but fall short in identifying crucial birth-related factors like preterm births (before the 37th week of gestation). Furthermore, distinguishing between stillbirth and livebirth is challenging, hindering the differentiation of these distinct life events.

From the skeletal elements, teeth possess a remarkable quality since they retain vital information throughout their formation. During this process, they capture and preserve crucial data, including the daily growth patterns of enamel, physiological stresses encountered during development, and even the chronological age at the time of an individual's death, in cases where crown completion had not occurred (Nava et al., 2017a, 2019, 2022; Smith and Tafforeau, 2008; Witzel et al., 2008).

Enamel formation is done by specialized cells called ameloblasts, following a specific pathway from the enamel-dentine junction (EDJ) to the outer enamel surface. This process adheres to a 24-h circadian rhythm, evident in primate enamel through daily incremental markings known as enamel cross-striations (Antoine et al., 2009; Kierdorf et al., 2021). Two types of lines in enamel provide insights into growth rhythm: periodic lines like Retzius Lines (RLs), influenced by ameloblast biological rhythm and possibly associated with weekly biological patterns (T. M. Smith et al., 2007), and non-periodic stress lines that appear in response to systemic disturbances during enamel formation, leading to the creation of Accentuated Lines (ALs). The Neonatal Line (NNL) is a distinctive AL that appears in the enamel of primary teeth after birth, this includes deciduous teeth as well as the first permanent mandibular molar (Antoine et al., 2009; Nava et al., 2017a). It is characterized by optical changes resulting from variations in the size, direction, and degree of mineralization of the enamel prisms. These alterations are caused by the biological stress imposed by the change from intrauterine to extrauterine life as well as changes in the quality and form of nutrition (Janardhanan et al., 2011; Kurek et al., 2016).

In the field of biological anthropology, the NNL plays a crucial role as a chronological marker of birth, distinguishing between prenatal and postnatal growth (Antoine et al., 2009). According to the literature, the NNL becomes visible in individuals who have survived for at least 10–15 days after birth, and potentially even earlier (Fitzgerald and Hillson, 2009; Schwartz et al., 2010; P. Smith and Avishai, 2005). It serves as a reference point for initiating the cross-striation count, necessary for calculating chronological age (Witzel, 2014). Therefore, unerupted and still-forming crown primary teeth provide a unique material for accurately determining the duration of an infant's survival by quantifying the amount of enamel tissue formation occurring after birth.

Traditionally, histological analysis has been used to identify the NNL (Hurnanen et al., 2017; Janardhanan et al., 2011; Kurek et al., 2016; Mahoney, 2011; Siebke et al., 2019; Zanolli et al., 2011). The NNL tends to be the first AL observed in the enamel (Hurnanen et al., 2017). It is distinguishable by its prominence and the clearer disruption in enamel prisms, which appears as a dark, sharp band against the lighter surrounding enamel when viewed under transmitted light microscope (Hurnanen et al., 2017; Kurek et al., 2016; Zanolli et al., 2011). Recent research has demonstrated the potential of Synchrotron X-ray Fluorescence (SXRF) for identifying the NNL by examining the distribution of zinc (Zn) and calcium (Ca) across the enamel and dentin layers of erupted deciduous teeth (Dean et al., 2019). They revealed a prominent Zn peak at NNL location which they attributed to the consistent and elevated levels of Zn during the initial 10 days of lactation. However, to our knowledge, this type of analysis has not been conducted with human archaeological tooth germs.

Previous studies have extensively investigated enamel formation and its relevance in estimating the age at death for infants (Mahoney, 2011, 2012, 2015). Some studies have given the age at death with archaeological deciduous teeth by direct counts of the cross-striations and the visualization of different biological marks as ALs (Kierdorf et al., 2021; Peripoli et al., 2023). Birch and Dean (2014) provided a regression formula to estimate enamel formation times, especially helpful when daily cross-striations aren't clear. Building upon this, Nava et al. (2017a) introduced a novel regression formula for estimating prenatal crown formation time (pCFT) based on direct counts of cross-striations along prisms. They derived the formula by statistically analyzing the relationship between the accumulated counts of cross-striations and the enamel thickness.

Tooth germs from infant individuals younger than one year are fragile and susceptible to taphonomic factors. This is because the enamel has not yet achieved its final high mineral content as it is still being affected by stress events of the secretory stage of amelogenesis that precedes the maturation stage (Kierdorf et al., 2009). This can make visualization of the NNL, cross-striations, and detection of elements in SXRF difficult. Additionally, the literature indicates that prenatal ALs can occur, complicating the analysis (FitzGerald and Saunders, 2005; Kierdorf et al., 2021; Nava et al., 2017b; Peripoli et al., 2023). Therefore, analyzing an archaeological sample of tooth germs presents substantial challenges.

Our study builds on previous research that has examined enamel formation and NNL identification in deciduous teeth (Birch and Dean, 2014; Dean et al., 2019; Kierdorf et al., 2009, 2021; Mahoney, 2011, 2012, 2015; Nava et al., 2017a; Peripoli et al., 2023). Our principal focus is accurately assessing the age of intramural inhumations of infant individuals during the Iberian Iron Age from histological sections of tooth germs. This will help us classify individuals within the different stages of infant mortality to reconstruct infant mortality patterns in Iberian Iron Age populations.

By accurately determining the age, this study will provide crucial insights into the reconstruction of life history and mortality patterns among infant burials in Iberian settlements dated to the Iron Age (8th-1st centuries BC). The Iberian culture inhabited the eastern and southern coastal regions of the Iberian Peninsula during the Iron Age. Their usual funerary ritual consisted of the cremation of the corpse and placing their ashes in urns, which were then buried in urnfields. Debate among researchers surrounds the practice of intramural inhumations of infants within buildings of domestic sites and in economic areas of production (Subirà and Molist, 2007). The reason for this funerary ritual is not understood, and the hypothesis comes from theoretical studies and interpretations (Afonso et al., 2019; Blasco Sancho and Montón Broto, 2019; Jener and Ortíz, 2008; Lorrio et al., 2010). A deep analysis of the biological profile of these infants had to be performed to get enough objective elements to achieve an accurate interpretation of these deaths.

2. Materials and methods

2.1. Tooth samples

This study analyses deciduous teeth from 45 infant skeletal remains excavated from five North-eastern Iberia settlements (Table 1 and Fig. 1). A total of 45 archaeological deciduous teeth were selected from the infant skeletal remains. Preferentially, upper central incisors were selected, considering their more advanced development during the time of birth. When these teeth were not available, deciduous lateral incisors or deciduous first molars were selected. To minimize the anthropological record damage, we analyzed one tooth per individual for the histological study (Supplementary Material 1).

Additionally, we analyzed two tooth germs from the Granada

Table 1
Sample of study. Site, abbreviation, chronology, and the number of individuals and teeth used in this study.

Provenance	Chronology	Reference	Code	Number Individuals
Fortress of Els Vilars	775 to 325 BC	López et al. (2021)	VILA	20
Olèrdola	350 to 200 BC	Subirà and Molist (2007)	OLE	7
Puig de Sant Andreu	350 to 280 BC	Martín (1985)	PDSA	3
Illa d'en Reixac	350 to 210 BC	Martín et al. (1989)	ILLA	3
Camp de les Lloses	125 to 75 BC	Duran et al. (2017)	CLENT	12
The Granada Osteological Collection of identified infants	20th century	Alemán et al. (2012)	G-	2

identified skeletal collection of infant individuals, housed at the Department of Legal Medicine, Toxicology and Physical Anthropology, of the University of Granada, Spain (Alemán et al., 2012). These teeth play a crucial role as reference samples due to their modern origin, the presence of NNL, and the availability of precise information regarding the chronological age.

The teeth were identified using the FDI World Dental Federation notation (ISO, 2016). Each tooth was measured and photographed (Liversidge et al., 1993; Hillson, 2005). Additionally, 3D photogrammetry models were created for archaeological teeth ensuring the creation of precise digital replicas that capture detailed tooth morphology.

2.2. Histological sections

The thin sections were obtained using a specific and customized approach based on previous methodologies (Caropreso et al., 2000; Silva et al., 2011). The teeth were embedded in acrylic mounting resin (ClaroCit Kit ®, Struers) and cut in the mid-sagittal plane using a Minitom (Struers) with a diamond cut-off wheel. The resulting sections were then attached to the mounting medium (Eukitt), and thin sections of 450-350 µm were obtained with the Minitom. To achieve an optimal thickness of 80–100 µm, 2000 µm P silicon carbide abrasive paper was used (Silva et al., 2011). The resulting section was dehydrated in ethanol (70%, 96%, and 100%), immersed in a histological clarifying agent (Histolemon, Carlo Erba Reagents S.A.S), and mounted with a coverslip using DPX mounting media (PanReac AppliChem ITW Reagents ®).

The histological sections were observed under a transmission petrographic optical microscope with a Leica DM2700 P dual polarisation system at 5X, 10X, and 20X magnifications, using Micrometrics SE Premium Software. Photocompositions of the images were created using MosaicJ (Schindelin et al., 2012).

2.3. Calculation of enamel daily secretion rate (DSR)

To analyze the histological image, preference was given to the buccal side of the tooth whenever possible, since it was the area that was best preserved and where the NNL was best visualized. In cases where the buccal side exhibited significant taphonomic alterations, the lingual side was used. Given that DSR cannot be calculated in all the prisms of all samples we have followed an alternative method to the direct counts to calculate the CFT. To facilitate accurate calculations, for each tooth we have calculated the average DSR in three different regions of the crown: upper, middle, and inferior (Fig. 2). This division was achieved by equally partitioning the length of the amelodentinal junction into three parts. Such an approach was necessary due to the diverse developmental stages of the tooth germs across the samples, precluding direct comparisons between regions of varying developmental states. This involved counting the daily incremental markings within the enamel prisms, following established methods outlined in the literature (Birch and Dean, 2014; Mahoney, 2012, 2015; Mahoney et al., 2016). For standardizing, we focused our analysis of the DSR on the mid-enamel area in each specified region (Mahoney et al., 2024). Specifically, the distance between three to five cross-striations was measured, and this distance was subsequently divided by the total number of cross-striations present. To ensure accuracy, between 15 and 20 measurements were conducted for each region, resulting in a total of 45–60 measurements per tooth. The 95% confidence interval (95CI) of the mean DRS was obtained for every region of the same tooth.

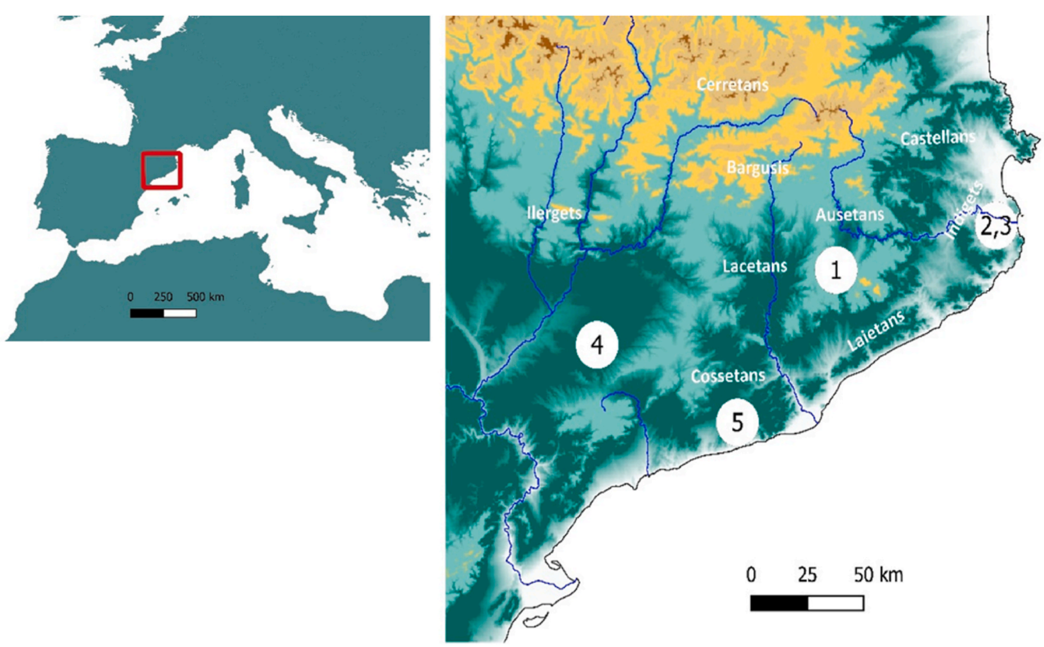

Fig. 1. Location map of the archaeological sites of North-eastern Iberia dated to the Iron Age included in this study: 1. Camp de les Lloses. 2. Illa d'en Reixac. 3. Puig de Sant Andreu. 4. Fortress of Els Vilars. 5. Olèrdola.

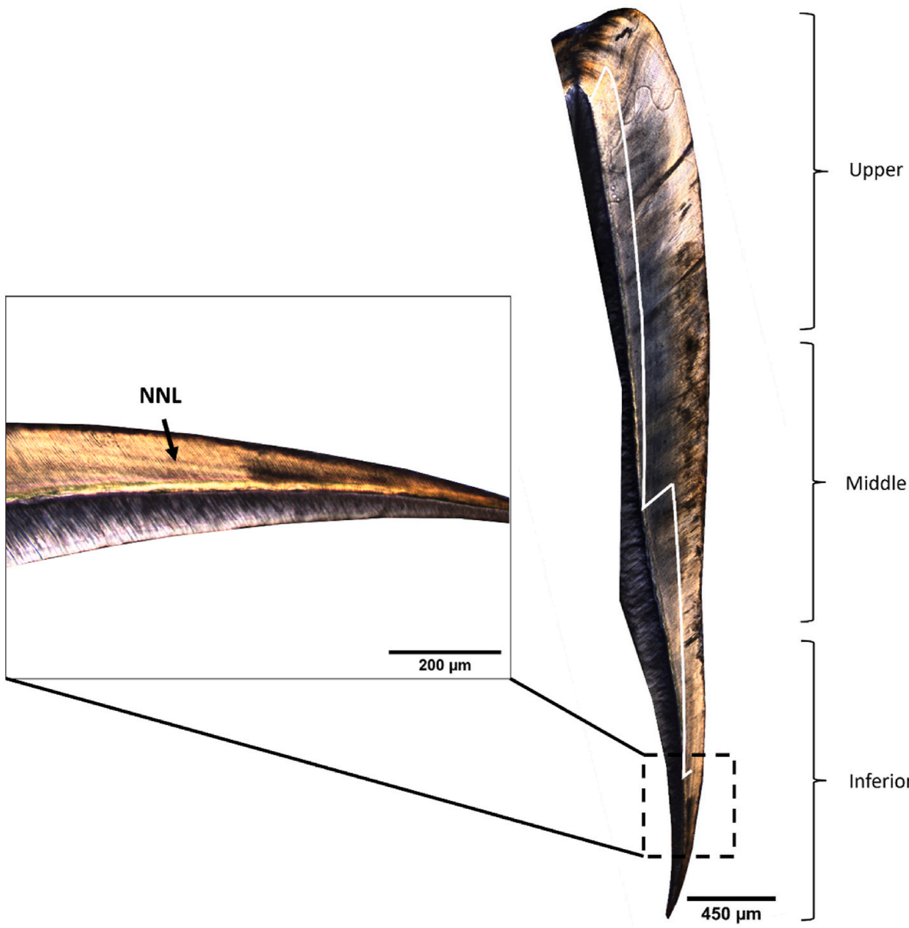

Fig. 2. Buccal side of the upper central incisor of individual OLE01, showing the upper, middle, and inferior enamel region. The white zigzag line that runs 200 μm from the EDJ and then back along the direction of the long-period RL shows the pCFT calculation. In the histological image at 10X, the NNL is indicated with an arrow.

2.4. Neonatal line (NNL) and crown formation time (CFT)

Initially, we conducted a comprehensive examination of the NNL in all samples to validate its presence. The NNL can be distinguished based on its characteristic features. Typically, the ALs differentiate from RLs because of the nature of the systemic trigger that produced them which histologically makes them visible along at least 75% of their length (FitzGerald and Saunders, 2005). The NNL tends to be the first AL and is usually more marked than other ALs, thus serving as a reliable marker for identification (Adserias-Garriga and Visnapuu, 2019). However, the first AL does not always align with the NNL (FitzGerald and Saunders, 2005; Kierdorf et al., 2021; Nava et al., 2017b; Peripoli et al., 2023) and based on our experience the distinction from other ALs is challenging in archaeological teeth.

To establish a more accurate distinction of the NNL, we calculated the pCFT, the time between the beginning of tooth enamel formation and the birth (marked by the NNL), following the works of (Nava et al., 2017a, 2017b; Peripoli et al., 2023). This method assumed a consistent time of crown initiation (18 weeks for central incisors, 20 for lateral incisors, and 19 for first molars) in humans and compared the pCFT values to documented ranges in existing literature based on the average duration of pregnancy, which is 39 weeks given as ages post menses (Mahoney, 2012, 2015; Birch and Dean, 2014). This determination was based on the presence of any discernible incremental pattern, whether it be an AL or RL running from the EDJ to the enamel surface, following Dean (2012). If no discernible incremental pattern was observable under polarized transmitted light the respective section was omitted from the analysis.

Determining pCFT involved tracing a 200 μm line from the EDJ along enamel prisms, forming a zig-zag pattern retraced along long-period RLs. This sequential tracing continues until reaching the NNL, allowing pCFT calculation. The 95 CI of the mean DSR for each zone (upper, middle, and inferior) and tooth has been used to calculate the days to form each 200 μm prism line, with the sum of these calculations providing maximum and minimum pCFT values. When the NNL is present, the chronological age of survival is calculated by measuring the prism length from the EDJ to the outer enamel surface and dividing it by the sample mean DSR (95 CI) in the specific region at the NNL-EDJ meeting point (Fig. 2). If NNL is absent, tracing extends throughout the whole crown.

2.5. Synchrotron X-ray fluorescence (SXRF) elemental analysis

To further validate the identification of the NNL and distinguish it from other accentuated stress lines (AL), two contemporary teeth from the Granada identified skeletal collection, and two archaeological samples were subjected to SXRF analysis. This study used the elemental composition of Zn, Ca, and Cu as they play critical roles in bone formation and metabolic processes, aiding in the identification of the NNL's location (Boldsen et al., 2024; Carvalho et al., 2007; Fischer et al., 2008; Wasowicz et al., 2001).

The sample preparation was done following the method described by Dean et al. (2019). The samples were mounted onto the Model 160 Specimen Grinder (E.A. Fischione Instruments) using Mounting Wax

(Allied High-Tech Products). This allowed us to polish the samples to 80 μm using 2000 μm P silicon carbide abrasive paper. Without dismounting it, the sample was subjected to a 10-min ultrasonic bath for additional cleaning. After the bath, the sample was carefully detached using heat with a Plactonic Hotplate (JP Selecta™). Subsequently, the sample was placed between Kapton films.

SXRF analysis was conducted in the BL13-XALOC beamline at the ALBA Synchrotron facility (Fauth et al., 2013; Juanhuix et al., 2014). The zones of interest within the polished thin section were measured using a transmission geometry setup, employing a focused beam with dimensions of 10×50 μm^2 and a photon energy of 12 keV (1.03320 Å).

A Pilatus 6M (Dectris) pixel array detector was utilized for data collection. This photon-counting detector provides a minimal noise level, a large dynamic range, and a large active area of 424×435mm^2 (equivalent to 6 megapixels). The fluorescence peaks of the elements of interest were characterized using an XFlash 410-SA fluorescence detector (Bruker) available at the beamline, typically employed for anomalous diffraction experiments and metal characterization in biological macromolecules.

We analyzed the ratios of the Kα emission lines between Zn and Cu with respect to Ca to examine the relationship between the specific element of interest and Ca concentrations within the dental samples. The size of the X-ray beam was 10 mm in the direction of the fluorescence scan, which had a sampling of 5 mm.

3. Results

3.1. Contemporary specimens

Analysis of contemporary samples is essential to validate the methodology before applying it to archaeological samples. Two contemporary samples (G-393, and G-399) underwent analysis using SXRF. For the deciduous lower central incisor of individual G-399, with a documented known age of 60 days, fluorescence ratio profiles of Zn/Ca and Cu/Ca were examined in two regions of the buccal side of the crown (Fig. 3a and b). A noticeable AL in enamel and dentine is observed in the first region (more proximal to the cusp). In the second region (more cervical), another AL is noticed in the enamel. In the dentin, an AL is also observed, but it corresponds to the same AL observed in the first region. Based on the pCFT and the survival age calculation, the NNL should correspond to the most cervical AL in enamel and the AL observed in dentin in both regions (Fig. 3a and b).

In the first region, coinciding with the enamel AL (Fig. 3a), a decrease in Ca levels is observed, while there are no significant changes in Zn and Cu levels. In dentin, a subtle increase of Zn is observed coinciding with the NNL. Ca and Cu levels remain without changes.

In the second region (Fig. 3b), a significant surge in Zn is noted in both the enamel and dentin coinciding with the NNL. In enamel, this increase in Zn coincides with increased Cu levels and a significant decrease in Ca.

We also analyzed a contemporary deciduous upper lateral incisor from individual G-393, with a documented known age of 91 days. Our analysis revealed an increase in Zn in both enamel and dentin NNL, as

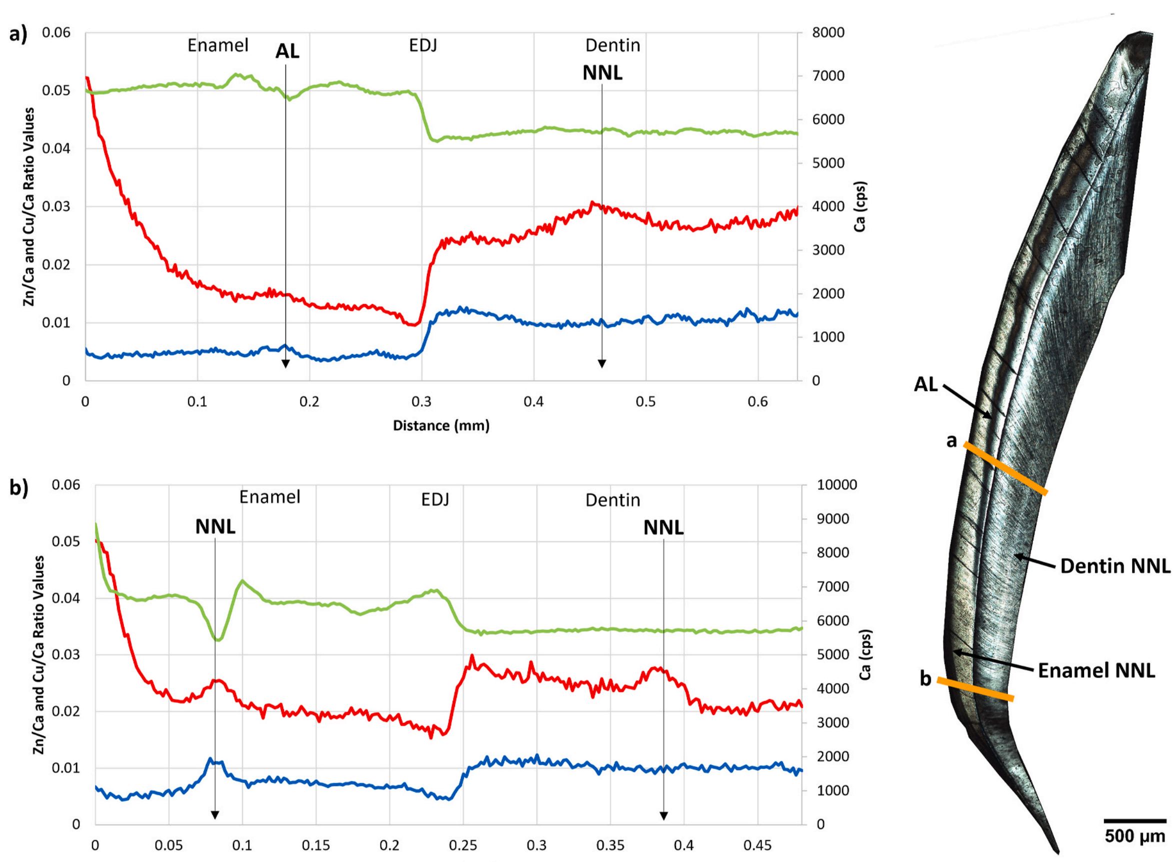

Fig. 3. Ratios of the intensity of Ka emission lines of zinc and copper with respect to calcium in XRF experiments of the lower deciduous incisor in sample G-399. The figure shows: a) a 1D line scan within the Accentuated Line (AL) in enamel and the NNL in dentine in the first region, b) a 1D scan line within the NNL in enamel and dentin in the second region. The ratio profiles of Zn/Ca (depicted in red) and Cu/Ca (depicted in blue), along with the counts per second (cps) of Ca (depicted in green), are presented. The photocomposition on the right displays the buccal side of the tooth, indicating the profile positions and orientations. (For interpretation of the references to colour in this figure legend, the reader is referred to the Web version of this article.)

well as an increase in Cu and a decrease in Ca specifically in the enamel (Fig. 4a).

3.2. Iberian specimens (8th-1st centuries BC)

The CFT was determined for 38 out of the 45 archaeological tooth sections (Figs. 5 and 6). Seven samples were excluded from the analysis due to issues such as fungus, bubbles, the loss of the two ends of the crown, or due to the lack of sufficiently clear incremental lines in the enamel for accurate calculations (Supplementary material, Table S1).

Out of the 38 tooth archaeological samples in which the CFT could be calculated, the NNL was not observed in 19 of them (archaeological samples depicted just with black boxes in Figs. 5 and 6).

Our histological examination of samples from individuals OLE03, VILA10, and CLENT09 revealed the presence of an AL. Because their CFT up to the AL falls below the expected range for full-term birth, we did not consider them as NNLs but as prenatal ALs and thus classified them as stillbirths.

We identified ten individuals with pCFT values lower than the established range for full-term birth and without NNL (samples depicted just with black boxes and below the gray frame in Figs. 5 and 6). Six of these individuals were born preterm (before the 37th week of gestation) since they present pCFT values at least 14 days lower than the established pCFT.

Seven individuals exhibited a pCFT within the established range for full-term birth (archaeological samples depicted just with black boxes

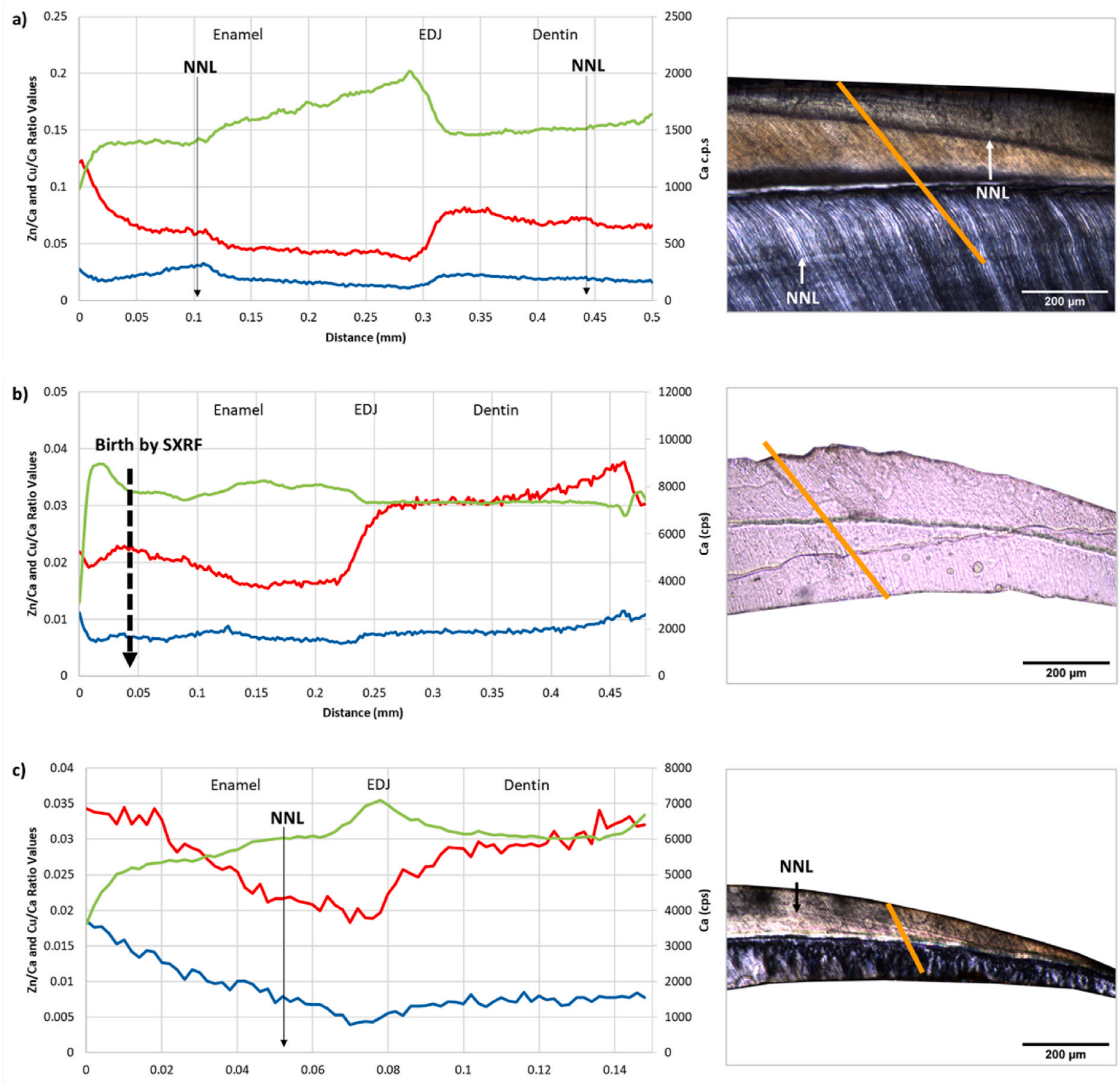

Fig. 4. Ratios of the intensity of Ka emission lines of zinc and copper with respect to calcium in XRF experiments. The figure shows: a) a graphical representation of the 1D line scan across the upper lateral deciduous incisor in sample G-393, illustrating the enamel and dentin's NNL, accompanied by a 10x magnified image detailing the profile's position, orientation, and indicating the NNL in enamel and dentin with arrows, b) a graphical representation of the 1D line scan across the upper central deciduous incisor in sample VILA15, accompanied by a 10x magnified image detailing the profile's position, and orientation, c) a graphical representation of the 1D scan line across the upper central deciduous incisor in sample VILA18 within the enamel and dentin, accompanied by a 10x magnified image indicating the profile's position, orientation, and indicating the NNL in enamel with an arrow. The ratio profiles of Zn/Ca (depicted in red) and Cu/Ca (depicted in blue), along with the counts per second (cps) of Ca (depicted in green), are presented. (For interpretation of the references to colour in this figure legend, the reader is referred to the Web version of this article.)

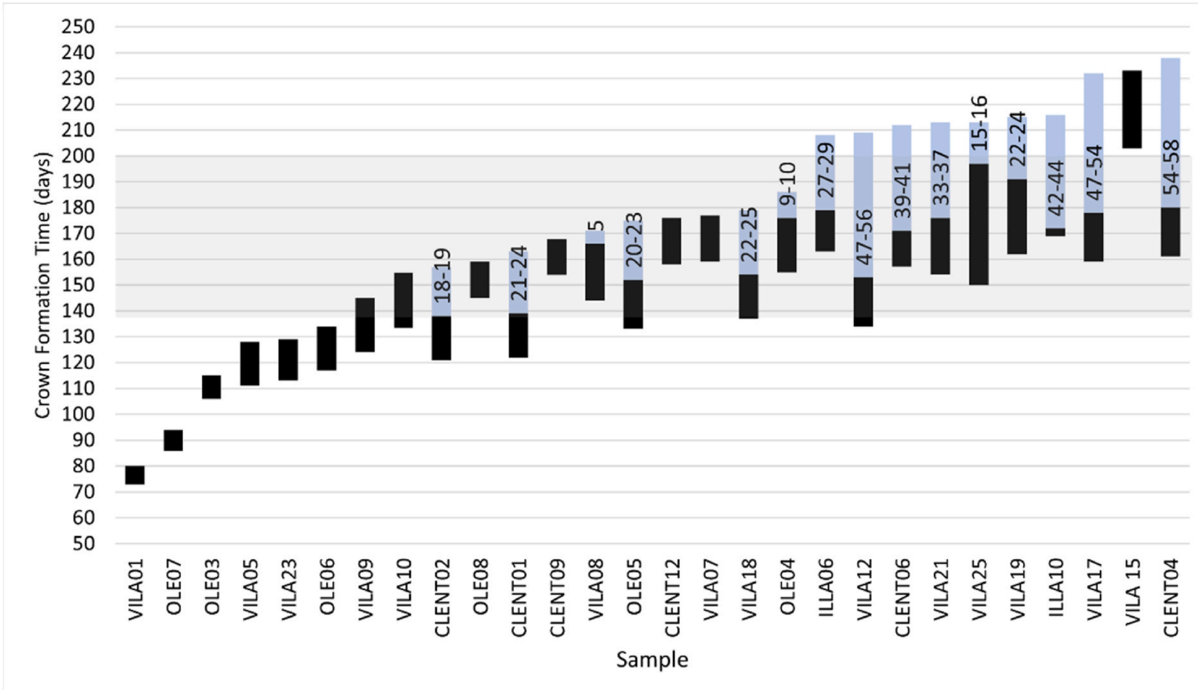

Fig. 5. Graphical representation of the Crown Formation Time (CFT) for the deciduous central incisor arranged in ascending order from the lowest to highest CFT. The gray frame encapsulates the published data on prenatal CFT (pCFT) between the 39 to 40 gestational weeks for central incisors (ranging from 137 to 201 days) as reported by Mahoney (2012, 2015) and Birch and Dean (2014). The pCFT (95CI) for each sample is depicted within black boxes. The survival periods in days (postnatal CFT 95CI) are indicated in blue boxes. (For interpretation of the references to colour in this figure legend, the reader is referred to the Web version of this article.)

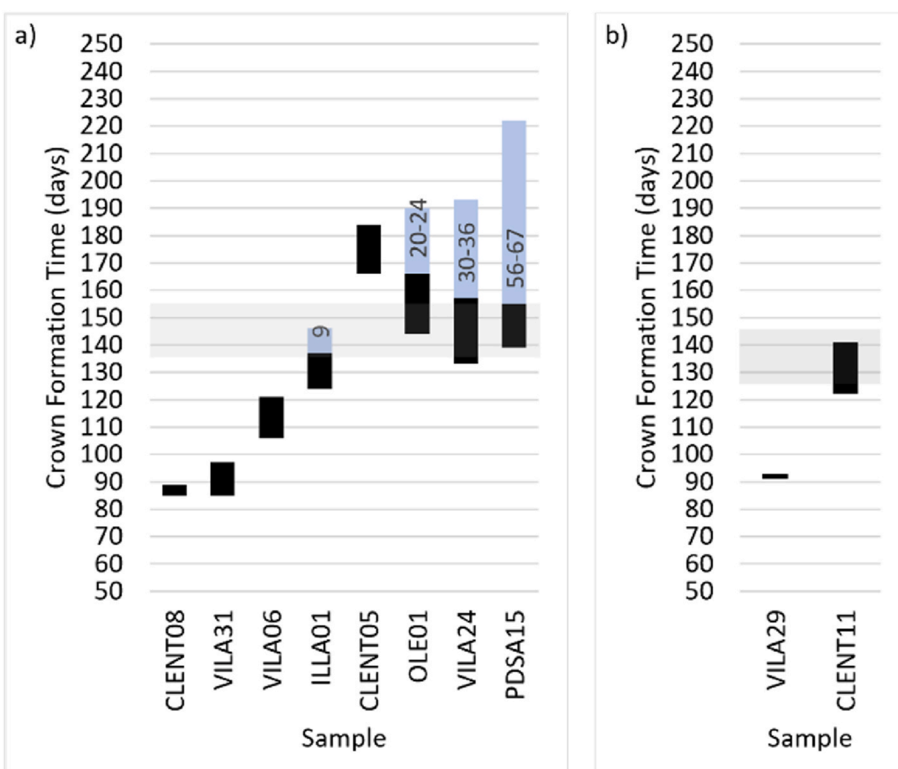

Fig. 6. Graphical representation of the Crown Formation Time (CFT) for the deciduous a) lateral incisor, and b) first molar samples, arranged in ascending order from the lowest to highest CFT. The gray frame encapsulates the published data on prenatal CFT (pCFT) between the 39 to 40 gestational weeks for a) lateral incisors (ranging from 136 to 156 days), and b) first molars (ranging from 125 to 146 days), as reported by Mahoney (2012, 2015) and Birch and Dean (2014). The pCFT (95CI) for each sample is depicted within black boxes. The survival periods in days (postnatal CFT 95CI) are indicated in blue boxes. (For interpretation of the references to colour in this figure legend, the reader is referred to the Web version of this article.)

and within the gray frame in Figs. 5 and 6). In the absence of a visible NNL, these individuals are considered full-term, yet stillbirths.

The tooth samples from individual VILA15 and CLENT05 did not exhibit NNL but their CFT value surpasses the reported range by a minimum of 2 and 10 days, respectively (Figs. 5 and 6). With this extended pCFT, these individuals were probably a livebirth, and the NNL was either not formed or not observable. In SXRF analysis with VILA15, an increase in Zn and Cu, alongside a decrease in Ca, was observed in the enamel but not in the dentin (Fig. 4b). With these results, we could calculate the survival age of 33–40 days (Fig. 5). Unfortunately, CLENT05 could not be analyzed by SXRF, as there was no sample available, but its estimated survival falls within the range of 1–28 days.

We were able to confirm that 19 individuals were indeed born at full-term, as their pCFT values fell within the established ranges, and NNL (Fig. 7) was observed (samples with blue boxes in Figs. 5 and 6). Calculated survival times span from 5 to 67 days. One of the samples (VILA18) was examined through SXRF to confirm the presence of the NNL. Conversely, no elemental changes were noted (Fig. 4c).

3.3. Infant mortality patterns

The mortality profile of infant individuals from Iron Age settlements of North-eastern Iberia has been determined through the study of the NNL and CFT (Fig. 8). An assumption has been made to reconstruct the mortality patterns of all Iberian infant sampled individuals. Some individuals classified as stillbirths might have survived for a few days postnatally, as the NNL becomes visible in individuals who have lived for at least 10–15 days after birth (Fitzgerald and Hillson, 2009; Schwartz et al., 2010; P. Smith and Avishai, 2005). Hence, individuals categorized as stillbirths and livebirths up to seven postnatal days (early neonatal period) have been grouped within the perinatal period.

In our Iberian sample, perinatal mortality (27th week of gestation to 7 days post-birth) constitutes almost half of the infant population (18 out of 38: 47%). Interestingly, within the perinatal mortality, six individuals were classified as preterm births (before the 37th week of gestation). Eleven individuals (29%) belong to the late neonatal mortality (deaths between the 8th and 28th day of life). Finally, the post-neonatal mortality (deaths occurring between the 28th day and the end of the first year of life) is constituted by nine individuals (24%). It must be noted that the oldest infant individual of the sample survived between 56 and 67 days (PDSA15).

4. Discussion

4.1. NNL identification and age determination

The challenge of distinguishing the NNL from nearby ALs has been discussed previously (Jakobsen, 1975). The position of the NNL varies depending on the tooth studied and the gestation length (Sabel et al., 2008). To establish a more definitive distinction between prenatal or postnatal ALs and the NNL, histological and SXRF analyses have been undertaken in 2 modern deciduous teeth from known-age individuals.

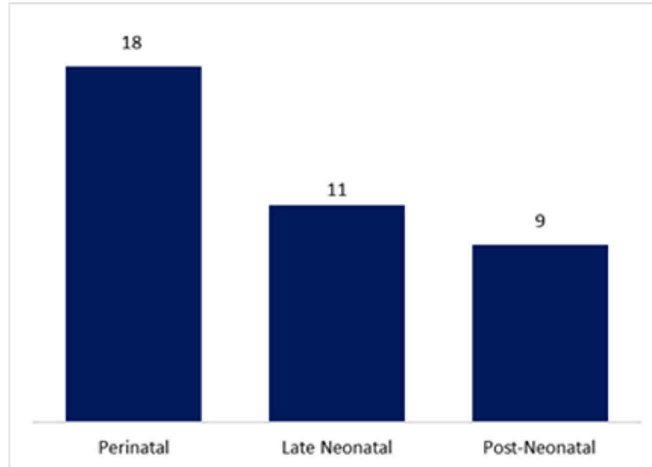

Fig. 8. Infant mortality profile of the individuals found in the Iberian Iron Age settlements. The data is divided into three mortality stages: Perinatal (27th week of gestation to 7 postnatal days), Late Neonatal (8th to 28th postnatal day), and Post-Neonatal (28th day to the first year of life).

SXRF analysis revealed an increase in Zn and Cu levels coupled with a decrease in Ca, in both NNLs from contemporary teeth with survival (see Figs. 3b and 4a). The tooth of individual G-399 showed two ALs (Fig. 3), being a prenatal AL the most apical and the NNL the most cervical. The SXRF analysis unveiled a decrease of Ca in both enamel ALs, with the most significant reduction observed at the NNL. At the prenatal AL element profile, there is a small Ca decline in the enamel. However, at the NNL element profile, this big disparity in Ca levels seems to be linked to symptomatic neonatal hypocalcemia experienced on the first day of life (Dean et al., 2019; Jaffe et al., 1973). At the first AL (more apical) there were no changes in Zn or Cu, whereas at the second one that coincides with the NNL, a noteworthy increase of Zn concentrations in both enamel and dentin and Cu concentration in enamel was revealed.

According to Dean et al. (2019), the high levels of Zn observed, particularly in breastfed infants, can be attributed to its enhanced incorporation into the still mineralizing enamel and dentin. This is because Zn is actively transported into breast milk via various types of zinc transporters in the mammary gland, a process that maintains a tightly regulated homeostasis (Lönnerdal, 2007). However, it is also worth noting that the concentration of Zn in milk decreases considerably during lactation, decreasing by up to 50% on the third day, with the highest concentration in the colostrum (Arnaud and Favier, 1992;

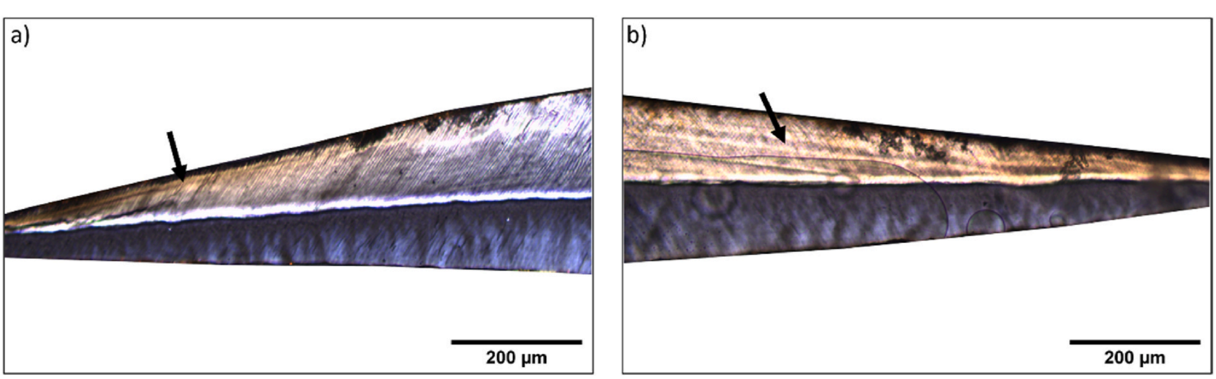

Fig. 7. Detailed histological images at 10X of the NNL indicated by black arrows: a) Central upper incisor from individual OLE04, b) Central lower incisor from individual OLE05.

Wasowicz et al., 2001). This decrease in Zn during lactation appears to align with the progressively decreasing demand and intake of Zn by the newborn (Nouzha et al., 2023). In contrast, non-breastfed infants may not exhibit higher Zn levels within the NNL (Dean et al., 2019).

Cu, like Zn, is another essential trace element that shows an increased concentration in women's blood during labour. This heightened concentration is influenced by factors beyond dietary intake, such as increased ceruloplasmin synthesis and elevated maternal estrogen levels (Mbofung and Atinmo, 1985; Wasowicz et al., 2001). In addition to these factors, copper mobilization from storage depots in various organs also contributes to the elevated concentration observed during labor (Thauvin et al., 1992). Similar to the trend observed with Zn, the concentration of Cu in milk also decreases during lactation (Nouzha et al., 2023; Wasowicz et al., 2001).

In our SXRF analysis of two archaeological tooth samples from the Iberian Iron Age period, we confirmed birth in VILA15 by the increase in Zn. Despite the absence of an observable NNL, its CFT exceeded the established range for full-term birth. Conversely, in VILA18 with an observable NNL, we were unable to confirm birth through elemental analysis. This highlights the utility of SXRF analysis with archaeological samples in confirming birth in cases where NNL cannot be observed by microscopy. However, this data must be approached cautiously. Even in samples where the NNL is visible (Fig. 3b) and the pCFT falls within the established range (Figs. 5 and 6) elemental changes confirming birth may not be evident. This might be due to the enrichment of zinc from the outer enamel surface reported in other studies (Brozou et al., 2023; Dean et al., 2023).

We verified survival to birth in 20 out of 38 individuals through CFT calculations and SXRF (Figs. 4–6). However, for those lacking observable or confirmed NNL, ensuring non-survival at birth is challenging, especially among individuals with pCFT values within the established range for full-term birth. This uncertainty raises the possibility of them passing away the first days after birth, necessary for the NNL formation. Additionally, it is important to consider potential individual variability in the onset of deciduous teeth mineralization in utero, which recent research suggests may be greater than previously assumed (Dean et al., 2020). Such variability could impact survival determinations, especially in the prenatal and perinatal periods, where small differences in mineralization timing may lead to misclassification.

4.2. *Infant mortality patterns during the Iron Age Iberia*

Through meticulous histological analysis of the examined tooth sample, we have effectively delineated the mortality patterns associated with intramural inhumations of infants found in Iron Age settlements (8th-1st centuries BC).

Infant mortality in low-income countries is a pressing issue that is influenced by a variety of interconnected factors. Preterm birth complications, pneumonia, birth asphyxia during labor, and malnutrition are the primary contributors to this problem (World Health Organization, 2021). As reported by the World Health Organization in 2021, the global neonatal mortality rate was 18 deaths per 1000 live births, with significant regional variations. In 1990, African nations reported an elevated rate of 86 deaths per 1000 live births. More recently, India had a rate of 32 deaths, while rural areas in Pakistan experienced an even higher rate of 62 deaths per 1000 live births (Jabeen et al., 2023; Pal et al., 2020).

The examination of the distribution of mortality by infant mortality stages (Fig. 8) in the Iberian sample revealed that perinatal mortality constitutes almost half (47%) of the sample. Notably, within this perinatal group, preterm infants were highly represented (6 out of 18 individuals). The prevalence of preterm births is a pertinent concern, with around 91% occurring in low and middle-income countries in 2015, primarily due to weaker health systems that struggle to provide essential family planning, antenatal care, and childbirth services (Okwaraji et al., 2023).

This global issue is compounded by the fact that preterm birth and its complications account for 35% of the estimated 3.1 million neonatal deaths worldwide, as preterm infants face heightened mortality and morbidity risks due to various mechanisms (Shah, 2015). In prehistoric times, the survival probability of preterm individuals would have been exceedingly low, considering that preterm birth is currently the leading cause of perinatal mortality, accompanied by long-term physical and neurodevelopmental effects (Okwaraji et al., 2023; Valentine et al., 2020).

Additionally, we found that out of the 20 full-term individuals who survived beyond one week, 11 (29%) were classified as late neonatal mortality, and 9 (24%) as post-neonatal mortality (Fig. 7). This aligns with the observed infant mortality patterns in contemporary societies (MacDorman et al., 2013; Valentine et al., 2020).

Our findings are in line with previous research on Iberian Iron Age samples, despite those studies having less precise age determination, smaller sample sizes, and no categorization of infant mortality stages, hindering comparative analysis (Afonso et al., 2019; Rissech et al., 2023). Their findings and ours suggest attritional mortality was common among infant intramural burials during the Iberian Iron Age.

However, it's important to note that while our study reveals a natural pattern of infant mortality, the age of these infants only extends up to two months of age. The oldest infant individual of the sample survived between 56 and 67 days. This discrepancy could potentially indicate a ritual selection within this specific age group. This is also found in similar archaeological contexts (Peripoli et al., 2023; Rissech et al., 2023).

5. Conclusions

This research presents a standardized procedure for reconstructing infant mortality patterns through the histological analysis of archaeological unerupted deciduous teeth. Accurate gestational and survival times at birth for infants were determined through CFT calculations and identification of the NNL. The SXRF analysis in contemporary tooth samples with known ages revealed a decrease in Ca concentrations and an increase in Zn and Cu concentrations coinciding with the enamel NNL. This pattern was also observed in one archaeological tooth, enabling age calculation even without a visible NNL. However, taphonomic factors affecting archaeological teeth can complicate the interpretation of SXRF analysis results. This underscores the need for further SXRF studies with archaeological tooth germs to ascertain the technique's utility in determining the NNL presence.

Our study enabled us to determine the chronological age of 38 individuals from the Iron Age Iberia, unveiling an attritional mortality pattern within these infant intramural burials. This study not only distinguishes mortality in various infant mortality stages but also effectively differentiates between stillbirth and livebirth, as well as preterm and full-term births. The presence of a notable number of preterm births within the perinatal stage supports the hypothesis of mortality primarily attributed to natural causes.

We anticipate further advancements in our research through future studies involving SXRF analysis with archaeological samples. This evolving research promises to unveil more intricate details about the lives and health of ancient populations, ultimately contributing to a more comprehensive understanding of human existence across different eras and civilizations.

CRediT authorship contribution statement

Ani Martirosyan: Writing – review & editing, Writing – original draft, Visualization, Methodology, Investigation, Formal analysis, Data curation, Conceptualization. **Carolina Sandoval-Ávila:** Writing – review & editing. **Javier Irurita:** Writing – review & editing, Resources. **Judith Juanhuix:** Writing – review & editing, Validation, Methodology, Formal analysis. **Nuria Molist:** Writing – review & editing, Resources.

Immaculada Mestres: Writing – review & editing, Resources. **Montserrat Durán:** Writing – review & editing, Resources. **Natàlia Alonso:** Writing – review & editing, Resources. **Cristina Santos:** Writing – review & editing, Resources, Project administration, Funding acquisition, Conceptualization. **Assumpció Malgosa:** Writing – review & editing, Supervision, Resources, Project administration, Funding acquisition, Conceptualization. **Judit Molera:** Writing – review & editing, Validation, Supervision, Resources, Methodology, Data curation, Conceptualization. **Xavier Jordana:** Writing – review & editing, Validation, Supervision, Resources, Project administration, Conceptualization.

Declaration of competing interest

The authors declare the following financial interests/personal relationships which may be considered as potential competing interests: Cristina Santos reports financial support was provided by Spain Ministry of Science and Innovation. Assumpcio Malgosa reports financial support was provided by Palarq Foundation. Assumpcio Malgosa reports financial support was provided by Government of Catalonia. If there are other authors, they declare that they have no known competing financial interests or personal relationships that could have appeared to influence the work reported in this paper.

Acknowledgments

The SXRF experiment was performed at BL-13 beamline at ALBA Synchrotron Light Facility with the collaboration of ALBA staff. The creation of the 3D models was made possible through the utilization of OpenLabs resources at the Universitat Autònoma de Barcelona. This research was supported by: Ministerio de Ciencia e Innovación (Ref. PGC2018-096666-B-100), Fundación Palarq (call for analysis 2022–2023; PALARQ23_55 Roma a l'Ausetània), Generalitat de Catalunya (GREAB research group, Ref. 2021 SGR 00186). Ani Martirosyan with a fellowship for predoctoral research staff in training (PIF) UAB. Xavier Jordana is a Serra Húnter Fellow of the Catalan university system. Special thanks to Patrick Mahoney for his feedback and review of earlier manuscript versions.

Appendix A. Supplementary data

Supplementary data to this article can be found online at https://doi.org/10.1016/j.jas.2024.106088.

References

Adserias-Garriga, J., Visnapuu, V., 2019. The neonatal line as evidence of live birth. In: Age Estimation: A Multidisciplinary Approach. Elsevier Inc. https://doi.org/10.1016/B978-0-12-814491-6.00011-X.

Afonso, C., Nociarova, D., Santos, C., Martinez-Labarga, C., Mestres, I., Duran, M., Malgosa, A., 2019. Sex selection in late Iberian infant burials: integrating evidence from morphological and genetic data. Am. J. Hum. Biol. 31 (1), 1–10. https://doi.org/10.1002/ajhb.23204.

Alemán, I., Irurita, J., Valencia, A.R., Martínez, A., Lõpez-Lázaro, S., Viciano, J., Botella, M.C., 2012. Brief communication: the Granada osteological collection of identified infants and young children. Am. J. Phys. Anthropol. 149 (4), 606–610. https://doi.org/10.1002/ajpa.22165.

Antoine, D., Hillson, S., Dean, M.C., 2009. The developmental clock of dental enamel: a test for the periodicity of prism cross-striations in modern humans and an evaluation of the most likely sources of error in histological studies of this kind. J. Anat. 214 (1), 45–55. https://doi.org/10.1111/j.1469-7580.2008.01010.x.

Arnaud, J., Favier, A., 1992. Determination of ultrafiltrable zinc in human milk by electrothermal atomic absorption spectrometry. The Analyst 117 (10), 1593–1598. https://doi.org/10.1039/an9921701593.

Birch, W., Dean, M.C., 2014. A method of calculating human deciduous crown formation times and of estimating the chronological ages of stressful events occurring during deciduous enamel formation. Journal of Forensic and Legal Medicine 22, 127–144. https://doi.org/10.1016/j.jflm.2013.12.002.

Blasco Sancho, M.F., Montón Broto, F.J., 2019. Enterramientos perinatales de la Primera Edad del Hierro en el poblado de La Codera (Alcolea de Cinca , Huesca). Bolskan 27, 41–54.

Boldsen, J.L., Dangvard, D., Milner, G.R., Kristensen, V.R.L., Skytte, L., Bergmann, S., Birk, T., Boje, C., Agersnap, L., Marie, I., Klingenberg, M., Krants, L., Mollerup, L., Seeberg, L., Christian, L., Morten, S., Kristensen, T., Tue, J., Baltzer, P., et al., 2024. Variation in Bioavailable Lead , Copper , and Strontium Concentrations in Human Skeletons from Medieval to Early Modern Denmark. https://doi.org/10.1016/j.jaa.2024.101587, 74(September 2023.

Brozou, A., Mannino, M.A., Van Malderen, S.J.M., Garrevoet, J., Pubert, E., Fuller, B.T., Dean, M.C., Colard, T., Santos, F., Lynnerup, N., Boldsen, J.L., Jørkov, M.L., Soficaru, A.D., Vincze, L., Le Cabec, A., 2023. Using SXRF and LA-ICP-TOFMS to explore evidence of treatment and physiological responses to leprosy in medieval Denmark. Biology 12 (2). https://doi.org/10.3390/biology12020184.

Caropreso, S., Bondioli, L., Capannolo, D., Cerroni, L., Macchiarelli, R., Condò, S.G., 2000. Thin sections for hard tissue histology: a new procedure. J. Microsc. 199 (3), 244–247. https://doi.org/10.1046/j.1365-2818.2000.00731.x.

Carvalho, M.L., Marques, A.F., Marques, J.P., Casaca, C., 2007. Evaluation of the diffusion of Mn, Fe, Ba and Pb in Middle Ages human teeth by synchrotron microprobe X-ray fluorescence. Spectrochimica Acta - Part B Atomic Spectroscopy 62, 702–706. https://doi.org/10.1016/j.sab.2007.02.011, 6–7 SPEC. ISS.

Dean, M.C., Garrevoet, J., Van Malderen, S.J.M., Santos, F., Mirazón Lahr, M., Foley, R., Le Cabec, A., 2023. The distribution and biogenic origins of zinc in the mineralised tooth tissues of modern and fossil hominoids: implications for life history, diet and taphonomy. Biology 12 (12), 1455. https://doi.org/10.3390/biology12121455.

Dean, M.C., Humphrey, L., Groom, A., Hassett, B., 2020. Variation in the timing of enamel formation in modern human deciduous canines. Arch. Oral Biol. 114 (February), 104719. https://doi.org/10.1016/j.archoralbio.2020.104719.

Dean, M.C., Spiers, K.M., Garrevoet, J., le Cabec, A., 2019. Synchrotron X-ray fluorescence mapping of Ca, Sr and Zn at the neonatal line in human deciduous teeth reflects changing perinatal physiology. Arch. Oral Biol. 104 (March), 90–102. https://doi.org/10.1016/j.archoralbio.2019.05.024.

Cunningham, C., Scheuer, L., Black, S., 2017. Developmental Juvenile Osteology, 2nd ed.

Dean, M.C., 2012. A histological method that can Be used to estimate the time taken to form the crown of a permanent tooth. In: Bell, En L. (Ed.), Forensic Microscopy for Skeletal Tissues. Methods and Protocols (Methods in Molecular Biology, vol. 915. Springer, pp. 89–100.

Duran, M., Mestres, I., Padrós, C., Principal, J., 2017. El Camp de les Lloses (Tona, Barcelona): evolución y significado del vicus romanorrepublicano. Roma En La Península Ibérica Presertoriana. Escenarios de Implantación Militar Provincial 56, 153–189.

Fauth, F., Peral, I., Popescu, C., Knapp, M., 2013. S360 vol. 28, No.S2, september 2013. Powder Diffr. 28 (September), 360–370.

Fischer, A., Kwapuliński, J., Wiechuła, D., Fischer, T., Loska, M., 2008. The occurrence of copper in deciduous teeth of girls and boys living in Upper Silesian Industry Region (Southern Poland). Sci. Total Environ. 389 (2–3), 315–319. https://doi.org/10.1016/j.scitotenv.2007.08.046.

Fitzgerald, C., Hillson, S., 2009. Deciduous tooth growth in an ancient Greek infant cemetery. Frontiers of Oral Biology 13, 178–183. https://doi.org/10.1159/000242414.

FitzGerald, C.M., Saunders, S.R., 2005. Test of histological methods of determining chronology of accentuated striae in deciduous teeth. Am. J. Phys. Anthropol. 127 (3), 277–290. https://doi.org/10.1002/ajpa.10442.

Hillson, S., 2005. Teeth. Cambridge Manuals in Archaeology. Cambridge University Press.

Hurnanen, J., Visnapuu, V., Sillanpää, M., Löyttyniemi, E., Rautava, J., 2017. Deciduous neonatal line: width is associated with duration of delivery. Forensic Sci. Int. 271, 87–91. https://doi.org/10.1016/j.forsciint.2016.12.016.

ISO, 2016. ISO 3950:2016 Dentistry — Designation System for Teeth and Areas of the Oral Cavity, fourth ed. International Organization for Standardization. Available at: https://www.iso.org/standard/68292.html.

Jabeen, S., Mushtaq, K., Samie, A., Hassan, S., 2023. Uncovering the rural–urban gap in determinants of infant mortality in Punjab-Pakistan. Sexual and Reproductive Healthcare 38 (September), 100918. https://doi.org/10.1016/j.srhc.2023.100918.

Jaffe, E.C., Stimmler, L., Osborne, J.A., 1973. Enamel defects associated with neonatal symptomatic hypocalcaemia. Proc. Br. Paedodontic Soc. 3 (0), 25–31.

Jakobsen, J., 1975. Neonatal lines in human dental enamel: occurrence in first permanent molars in males and females. Acta Odontol. Scand. 33 (2), 95–106. https://doi.org/10.3109/00016357509026348.

Janardhanan, M., Umadethan, B., Biniraj, K., Vinod Kumar, R., Rakesh, S., 2011. Neonatal line as a linear evidence of live birth: estimation of postnatal survival of a new born from primary tooth germs. J. Forensic Dent. Sci. 3 (1), 8. https://doi.org/10.4103/0975-1475.85284.

Jener, F., Ortíz, S., 2008. Panorama actual de la investigación de las inhumaciones infantiles en la protohistoria del sudoeste mediterráneo europeo. Nasciturus, Infans, Puerulus Vobis Mater Terra : La Muerte En La Infancia 257–329.

Juanhuix, J., Gil-Ortiz, F., Cuní, G., Colldelram, C., Nicolás, J., Lidón, J., Boter, E., Ruget, C., Ferrer, S., Benach, J., 2014. Developments in optics and performance at BL13-XALOC, the macromolecular crystallography beamline at the Alba Synchrotron. J. Synchrotron Radiat. 21 (4), 679–689. https://doi.org/10.1107/S160057751400825X.

Kierdorf, H., Kierdorf, U., Witzel, C., Intoh, M., Dobney, K., 2009. Developmental defects and postmortem changes in archaeological pig teeth from Fais Island, Micronesia. J. Archaeol. Sci. 36 (7), 1637–1646. https://doi.org/10.1016/j.jas.2009.03.028.

Kierdorf, H., Witzel, C., Bocaege, E., Richter, T., Kierdorf, U., 2021. Assessment of physiological disturbances during pre- and early postnatal development based on microscopic analysis of human deciduous teeth from the Late Epipaleolithic site of Shubayqa 1 (Jordan). Am. J. Phys. Anthropol. 174 (1), 20–34. https://doi.org/10.1002/ajpa.24156.

Kurek, M., Zadzińska, E., Sitek, A., Borowska-Strugińska, B., Rosset, I., Lorkiewicz, W., 2016. Neonatal line width in deciduous incisors from Neolithic, mediaeval and modern skeletal samples from north-central Poland. Ann. Anat. 203, 12–18. https://doi.org/10.1016/j.aanat.2015.02.006.
Liversidge, H.M., Dean, M.C., Molleson, T.I., 1993. Increasing human tooth length between birth and 5.4 years. Am. J. Phys. Anthropol. 90 (3), 307–313. https://doi.org/10.1002/ajpa.1330900305.
Lönnerdal, B., 2007. Trace element transport in the mammary gland. Annu. Rev. Nutr. 27, 165–177. https://doi.org/10.1146/annurev.nutr.27.061406.093809.
López, J.B., Junyent, E., Alonso, N., 2021. Architecture, power and everyday life in the iron age of NorthNorth-eastern Iberia. Research from 1985 to 2019 on the tell-like fortress of els Vilars (arbeca, lleida, Spain). Current Approaches to Tells in the Prehistoric Old World 189–208. https://doi.org/10.2307/j.ctv13pk5j9.15.
Lorrio, A.J., de Miguel, M.P., Moneo, T., Sánchez de Prado, M. a D., 2010. Enterramientos infantiles en el oppidum de El Molón (Camporrobles, Valencia). Cuadernos de Arqueología 18, 201–262.
Luke, B., Williams, C., Minogue, J., Keith, L., 1993. The changing pattern of infant mortality in the US: the role of prenatal factors and their obstetrical implications. Int. J. Gynecol. Obstet. 40 (3), 199–212. https://doi.org/10.1016/0020-7292(93)90832-H.
MacDorman, M.F., Hoyert, D.L., Mathews, T.J., 2013. Recent Declines in Infant Mortality in the United States, 2005-2011, vol. 120. NCHS Data Brief, pp. 1–8.
Mahoney, P., 2011. Human deciduous mandibular molar incremental enamel development. Am. J. Phys. Anthropol. 144 (2), 204–214. https://doi.org/10.1002/ajpa.21386.
Mahoney, P., 2012. Incremental enamel development in modern human deciduous anterior teeth. Am. J. Phys. Anthropol. 147 (4), 637–651. https://doi.org/10.1002/ajpa.22029.
Mahoney, P., 2015. Dental fast track: prenatal enamel growth, incisor eruption, and weaning in human infants. Am. J. Phys. Anthropol. 156 (3), 407–421. https://doi.org/10.1002/ajpa.22666.
Mahoney, P., McFarlane, G., Taurozzi, A.J., Madupe, P.P., O'Hara, M.C., Molopyane, K., Cappellini, E., Hawks, J., Skinner, M.M., Berger, L., 2024. Human-like enamel growth in Homo naledi. American Journal of Biological Anthropology, December 2023, 1–14. https://doi.org/10.1002/ajpa.24893.
Mahoney, P., Miszkiewicz, J.J., Pitfield, R., Schlecht, S.H., Deter, C., Guatelli-Steinberg, D., 2016. Biorhythms, deciduous enamel thickness, and primary bone growth: a test of the Havers-Halberg Oscillation hypothesis. J. Anat. 228 (6), 919–928. https://doi.org/10.1111/joa.12450.
Martín, M.A., 1985. Memòria de les campanyes d'excavació 1984 i 1985 en el Puig de Sant Andreu d'Ullastret (Baix Empordà). Generalitat de Catalunya, Barcelona.
Martín, M.A., Pons, E., López, J.B., Mataró, M., 1989. Memòria d'Excavació 1987-1989 de l'Illa d'en Reixac (Ullastret, Baix Empordà). Generalitat de Catalunya. Barcelona.
Mbofung, C.M.F., Atinmo, T., 1985. Zinc, copper and iron concentrations in the plasma and diets of lactating Nigerian women. Br. J. Nutr. 53 (3), 427–439. https://doi.org/10.1079/bjn19850052.
Monnier, A., 1985. Les méthodes d'analyse de la mortalité infantile. In: Pressat, En R. (Ed.), Manuel d'Analyse de la Mortalité. Institut National d'Études démographiques, Paris, pp. 47–59.
Nava, A., Bondioli, L., Coppa, A., Dean, C., Rossi, P.F., Zanolli, C., 2017a. New regression formula to estimate the prenatal crown formation time of human deciduous central incisors derived from a Roman Imperial sample (Velia, Salerno, Italy, I-II cent. CE). PLoS One 12 (7), 1–21. https://doi.org/10.1371/journal.pone.0180104.
Nava, A., Coppa, A., Coppola, D., Mancini, L., Dreossi, Di, Zanini, F., Bernardini, F., Tuniz, C., Bondioli, L., 2017b. Virtual histological assessment of the prenatal life history and age at death of the Upper Paleolithic fetus from Ostuni (Italy). Sci. Rep. 7 (1), 1–10. https://doi.org/10.1038/s41598-017-09773-2.
Nava, A., Frayer, D.W., Bondioli, L., 2019. Longitudinal analysis of the microscopic dental enamel defects of children in the Imperial Roman community of Portus Romae (necropolis of Isola Sacra, 2nd to 4th century CE, Italy). J. Archaeol. Sci.: Reports 23, 406–415. https://doi.org/10.1016/j.jasrep.2018.11.007. September 2018.
Nava, A., Mahoney, P., Bondioli, L., Coppa, A., Cristiani, E., Fattore, L., McFarlane, G., Dreossi, D., Mancini, L., 2022. Virtual histology of archaeological human deciduous prenatal enamel through synchrotron X-ray computed microtomography images. J. Synchrotron Radiat. 29, 247–253. https://doi.org/10.1107/S160057752101208X.
Nouzha, D.O., Louise, G., Claudia, S.B., Héloïse, F.M., Laurence, L., Joël, P., Virginie, R., 2023. Trace elements status in human breast milk of mothers from Île-de-France region. J. Trace Elem. Med. Biol. 80 (October), 1–7. https://doi.org/10.1016/j.jtemb.2023.127317.
Okwaraji, Y.B., Krasevec, J., Bradley, E., Conkle, J., Stevens, G., Gatica-Domínguez, G., Ohuma, E.O., Coffey, C., Estevez Fernandez, D., Blencowe, H., Kimathi, B., Moller, A.-B., Lewin, A., Hussain-Alkhateeb, L., Dalmiya, N., Lawn, J.E., Borghi, E., Hayashi, C., 2023. National, regional, and global estimates of low birthweight in 2020, with trends from 2000: a systematic analysis. Lancet 402, 1261–1271.
Pal, A., Yadav, J., Kumari, D., Jitenkumar Singh, K., 2020. Gender differentials and risk of infant and under five mortality in India. A comparative survival analysis. Child. Youth Serv. Rev. 118 (September), 105477. https://doi.org/10.1016/j.childyouth.2020.105477.
Peripoli, B., Gigante, M., Mahoney, P., McFarlane, G., Coppa, A., Lugli, F., Lauria, G., Bondioli, L., Sconzo, P., Sineo, L., Nava, A., 2023. Exploring prenatal and neonatal life history through dental histology in infants from the Phoenician necropolis of Motya (7th–6th century BCE). J. Archaeol. Sci.: Reports 49 (February), 104024. https://doi.org/10.1016/j.jasrep.2023.104024.
Razzaque, A., Chowdhury, R., Mustafa, A.G., Begum, F., Shafique, S., Lawton, A., Islam, M.Z., 2022. Levels, trends and socio-demographic determinants of infant and under-five mortalities in and around slum areas of Dhaka city, Bangladesh. SSM - Population Health 17 (January), 101033. https://doi.org/10.1016/j.ssmph.2022.101033.
Rissech, C., Witzel, C., Guardia, M., López-Costas, O., Götherström, A., Krzewińska, M., Kırdök, E., Mendiela, S., Merino, M., Francès, J., 2023. Skeletal remains of human perinatal individuals from the fortified Iberian Period settlement of Ca n'Oliver (6th century to 50 years BCE). Archaeological and Anthropological Sciences 15 (10), 1–28. https://doi.org/10.1007/s12520-023-01863-9.
Sabel, N., Johansson, C., Kühnisch, J., Robertson, A., Steiniger, F., Norén, J.G., Klingberg, G., Nietzsche, S., 2008. Neonatal lines in the enamel of primary teeth-A morphological and scanning electron microscopic investigation. Arch. Oral Biol. 53 (10), 954–963. https://doi.org/10.1016/j.archoralbio.2008.05.003.
Schindelin, J., Arganda-Carreras, I., Frise, E., Kaynig, V., Longair, M., Pietzsch, T., Preibisch, S., Rueden, C., Saalfeld, S., Schmid, B., Tinevez, J.Y., White, D.J., Hartenstein, V., Eliceiri, K., Tomancak, P., Cardona, A., 2012. Fiji: an open-source platform for biological-image analysis. Nat. Methods 9 (7), 676–682. https://doi.org/10.1038/nmeth.2019.
Schwartz, J.H., Houghton, F., Macchiarelli, R., Bondioli, L., 2010. Skeletal remains from punic carthage do not support systematic sacrifice of infants. PLoS One 5 (2), 1–12. https://doi.org/10.1371/journal.pone.0009177.
Shah, R., 2015. Preterm Birth : Risk , Care Seeking and Mortality in Bangladesh. October 2014.
Siebke, I., Moghaddam, N., Cunningham, C.A., Witzel, C., Lösch, S., 2019. Those who died very young—inferences from δ15N and δ13C in bone collagen and the absence of a neonatal line in enamel related to the possible onset of breastfeeding. Am. J. Phys. Anthropol. 169 (4), 664–677. https://doi.org/10.1002/ajpa.23847.
Silva, G.A.B., Moreira, A., Alves, J.B., 2011. Histological processing of teeth and periodontal tissues for light microscopy analysis. Methods Mol. Biol. 689, 19–36. https://doi.org/10.1007/978-1-60761-950-5_2.
Smith, P., Avishai, G., 2005. The use of dental criteria for estimating postnatal survival in skeletal remains of infants. J. Archaeol. Sci. 32 (1), 83–89. https://doi.org/10.1016/j.jas.2004.06.008.
Smith, T.M., Reid, D.J., Dean, M.C., Olejniczak, A.J., Ferrell, R.J., Martin, L.B., 2007. New perspectives on chimpanzee and human molar crown development. Vertebrate Paleobiology and Paleoanthropology 9781402058448, 177–192. https://doi.org/10.1007/978-1-4020-5845-5_12.
Smith, T.M., Tafforeau, P., 2008. New visions of dental tissue research: tooth development, chemistry, and structure. Evol. Anthropol. 17 (5), 213–226. https://doi.org/10.1002/evan.20176.
Subirà, M.E., Molist, N., 2007. Inhumacions perinatals múltiples i espais de treball en els assentaments ibers. Nasciturus: Infans, Puerulus. Vobis Mater Terra. La Muerte En La Infancia, Uh 4, 365–385.
Thauvin, E., Fusselier, M., Arnaud, J., Faure, H., Favier, M., Coudray, C., Richard, M.J., Favier, A., 1992. Effects of a multivitamin mineral supplement on zinc and copper status during pregnancy. Biol. Trace Elem. Res. 32 (1–3), 405–414. https://doi.org/10.1007/BF02784626.
Valentine, G.C., Chiume, M., Hagan, J., Kazembe, P., Aagaard, K.M., Patil, M., 2020. 55: neonatal mortality rates in the neonatal intensive care unit at kamuzu central hospital in Malawi. Am. J. Obstet. Gynecol. 222 (1), S45–S46. https://doi.org/10.1016/j.ajog.2019.11.071.
Wasowicz, W., Gromadzinska, J., Szram, K., Rydzynski, K., Cieslak, J., Pietrzak, Z., 2001. Selenium, zinc, and copper concentrations in the blood and milk of lactating women. Biol. Trace Elem. Res. 79 (3), 221–233. https://doi.org/10.1385/BTER:79:3:221.
Witzel, C., 2014. Echoes from birth - mutual benefits for physical and forensic anthropology by applying increment counts in enamel of deciduous teeth for aging. Anthropol. Anzeiger 71 (1–2), 87–103. https://doi.org/10.1127/0003-5548/2014/0386.
Witzel, C., Kierdorf, U., Schultz, M., Kierdorf, H., 2008. Insights from the inside: histological analysis of abnormal enamel microstructure associated with hypoplastic enamel defects in human teeth. Am. J. Phys. Anthropol. 136 (4), 400–414. https://doi.org/10.1002/ajpa.20822.
World Health Organization, 2021. Levels and trends in child mortality: report 2021. Retrieved from. https://www.who.int/news-room/fact-sheets/detail/levels-and-trends-in-child-mortality-report-2021.
Zanolli, C., Bondioli, L., Manni, F., Rossi, P., Macchiarelli, R., 2011. Gestation length, mode of delivery, and neonatal line-thickness variation. Hum. Biol. 83 (6), 695–713. https://doi.org/10.3378/027.083.0603.